A large sample investigation of temporal scale-invariance in rainfall over the tropical urban island of Singapore

Mandapaka, Pradeep V.; Qin, Xiaosheng

2014

Mandapaka, P. V., & Qin, X. A large sample investigation of temporal scale-invariance in rainfall over the tropical urban island of Singapore. Theoretical and applied climatology, in press.

https://hdl.handle.net/10356/79457

https://doi.org/10.1007/s00704-014-1317-6

Theoretical and Applied Climatology manuscript No.
(will be inserted by the editor)

A large sample investigation of temporal scale-invariance in rainfall over the tropical urban island of Singapore

Pradeep V. Mandapaka · Xiaosheng Qin

Received: date / Accepted: date

Abstract Scaling behavior of rainfall time series is characterized using monofractal, spectral and multifractal frameworks. The study analyzed temporal scale-invariance of rainfall in the tropical island of Singapore using a large dataset comprising 31 years of hourly and 3 years of 1-minute rainfall measurements. First, the rainfall time series is transformed into an occurrence–non-occurrence binary series, and its scaling behavior is analyzed using box-counting analysis. The results indicated that the rainfall support displays fractal structure, but within a limited range of scales. The rainfall support has a fractal dimension (D_f) of 0.56 for scales ranging from 1 minute to 1.5 h and a D_f of 0.37 from 1.5 h to 1.5 days. The results further showed that the fractal dimension decreases with the increase in the threshold used to define binary series. Spectral analysis carried out on the rainfall time series and the corresponding binary series showed three distinct scaling

P.V. Mandapaka · X.S. Qin (Corresponding author)

School of Civil and Environmental Engineering

50 Nanyang Avenue, Nanyang Technological University, Singapore 639798

Tel.: +65-67905288; E-mail: xsqin@ntu.edu.sg

regimes of 4 minute - 2h, 2 h - 24 h, and 24 h - 1 month. In all the scaling regimes, the spectral exponents for the rainfall series were smaller than those for the binary series. The study then investigated the presence of multiscaling behavior in rainfall time series using moment scaling analysis. The results confirmed that the rainfall fluctuations display a multiscaling structure, which was modelled in the framework of universal multifractals. The results from this study would not only improve our understanding of the temporal rainfall structure in Singapore and the surrounding Maritime Continent, but also help us build and parameterize parsimonious models and statistical downscaling techniques for rainfall in this region.

Keywords Fractal Dimension · Power spectrum · Multifractals · Universal Model · Maritime continent

1 Introduction

Characterization of intermittency and high degree of variability that rainfall displays in space and time is important for various applications in earth sciences. Scale-invariance (or scaling) provides an elegant framework to analyze and model rainfall characteristics across a range of temporal and spatial scales. A physical process is said to be scale-invariant, if large scale and small scale structures are related by a power-law that involves only the scale ratio and an exponent (e.g., Schertzer and Lovejoy, 1987). Many studies in the last three decades have shown empirical evidence of scaling in rainfall (e.g., Lovejoy, 1982; Fraedrich and Larnder, 1993; Georgakakos et al, 1994; Venugopal et al, 1999; Deidda et al, 2004; Lovejoy et al, 2008; Mandapaka et al, 2009; Rysman et al, 2013), and proposed models that can be used for generating synthetic rainfall fields or for obtaining

high resolution fields through downscaling (e.g., Lovejoy and Mandelbrot, 1985; Schertzer and Lovejoy, 1987; Over and Gupta, 1996; Deidda et al, 2004; Mascaro et al, 2014). Early studies were based on monofractal framework, where the variability is characterized by a single exponent (e.g., Lovejoy and Mandelbrot, 1985). The monofractal approach was soon generalized to a more unified multifractal framework to adequately describe intensity fluctuations across scales (e.g., Schertzer and Lovejoy, 1987).

Several studies employed multifractal analysis techniques to characterize variability of rainfall for temporal scales ranging from seconds to years (e.g., Olsson, 1995; Svensson et al, 1996; Pathirana et al, 2003; Mandapaka et al, 2009; Verrier et al, 2011; Yonghe et al, 2013), and spatial scales varying from meters to continental scales (e.g., Tessier et al, 1993; Gebremichael et al, 2008; Lovejoy et al, 2008; Mandapaka et al, 2009, 2010). However, very few studies investigated scale-invariance of rainfall in the Maritime continent, which consists of many densely populated and highly urbanized regions (e.g., Sivakumar, 2000a,b). These regions require high resolution (e.g., sub-hourly) rainfall time series for better modeling of urban hydrologic response. However, rainfall databases from many countries in the Maritime Continent are of coarse resolution. This study is motivated by our long-term goal to build parsimonious statistical downscaling models of rainfall and generate an ensemble of sub-hourly rainfall time series at multiple locations within the Maritime Continent.

An important step towards aforementioned goal is to investigate the presence of scale-invariance in temporal rainfall in the Maritime Continent, and characterize corresponding scaling regimes. Previous studies on rainfall scale-invariance in this region were based on limited sample size, where data resolution was too coarse

to analyse urban hydrologic scales (e.g., Sivakumar, 2000a,b). In this study, we take advantage of the availability of large dataset from a dense gauge network in Singapore to investigate the presence of scale-invariance in rainfall. The dataset consists of 31 years of hourly and 3 years of high-resolution 1-minute rainfall observations. We employ box-counting analysis (e.g., Lovejoy et al, 1987) to study the distribution of rainfall occurrence in time, and proceed to spectral (e.g., Fraedrich and Larnder, 1993) and multifractal analyses (e.g., Schertzer and Lovejoy, 1987) to study rainfall intensity fluctuations. To the best of our knowledge, this study is the first comprehensive investigation on the presence of scale-invariance in rainfall in a maritime continental region using multiple analysis techniques. The current study therefore complements the earlier work by Sivakumar (2000a,b), who analyzed 6-hourly rainfall data for the same region, although for a different time period.

A brief description of the study area and the rainfall data is provided in section 2. Section 3 describes the analysis tools and the metrics used to investigate scale-invariance in rainfall. The results are discussed in section 4 followed by concluding remarks in section 5.

2 Study Area and Data Description

Singapore is a tropical island nation extending from 1.16°N - 1.48°N and 103.6°E - 104.09°E, with an area $\sim$ 710 km^2 (Figure 1). There is no pronounced variability in topography, with most of the island at about 15 m above sea level. The highest point is the Bukit Timah hill at 164 m above sea level near the center of the island. The island is characterized by equatorial climate with high humidity, heavy

rainfall, and uniformly warm temperatures throughout the year (e.g., Fong, 2012). The average daily relative humidity varies from about 84% in March to 88% in December, and the average daily temperature ranges from 25.5°C in December–January to 27.3°C in May (e.g., Chia and Foong, 1991). The average annual rainfall is about 2400 mm with approximately 51% of rainy days (e.g., Mandapaka and Qin, 2013). Singapore experiences two monsoons: the southwest monsoon from June to september, and northeast monsoon from late November to March. The prevailing winds are from south-southeast direction during the southwest monsoon, and north-northeast direction during the northeast monsoon (e.g., Fong, 2012). The first half of the Northeast monsoon (December and January) is the wettest period of the year, and the second half (February in particular) is relatively dry. In addition, the period characterized by the southwest monsoon is drier compared to the northeast monsoon (e.g., Fong, 2012; Mandapaka and Qin, 2013).

In general, rainstorms in Singapore are convective in nature and rarely last longer than 1 to 1.5 h (Watts, 1955; Chatterjea, 1998, 2011). However these rainstorms are frequent and intense thus maintaining high monthly totals throughout the year. During the first half of the northeast monsoon, the convective storms are further intensified by the surges in low-level northeasterlies resulting in long duration wet spells and high monthly accumulations. A key feature of southwest monsoon is the Sumatra Squall, which is a line of thunderstorms that develops over the Strait of Malacca and reaches western coast of Peninsular Malaysia and Singapore around predawn hours or morning. Typical characteristics of a Sumatra Squall are intense rainfall for about 1 to 2 h, strong wind gusts and a sudden fall of temperature (e.g., Chia and Foong, 1991; Fong, 2012).

We analyse 31 years (January 1980 - December 2010) of hourly data from 49 stations and 3 years (July 2010 - June 2013) of 1-minute data from 5 stations in Singapore (Figure 1). The availability of such high-resolution data for such a long time period is unique for this region and allows us to investigate the presence of scaling relationships, which can be used to build statistical downscaling tools (e.g., Gaume et al, 2007; Licznar et al, 2011; Mascaro et al, 2014). It should be noted that in the hourly dataset, the type of the gauge used at some stations changed between the years 1980 and 2010. For example, all the stations in the year 1980 were equipped with recording type gauges with rain gauge charts attached. The precision of these gauges is 0.1 mm. By the year 2010, 20 out of 49 stations were equipped with tipping bucket gauges recording the number of 0.2 mm tips every minute. The hourly dataset has been used recently by Mandapaka and Qin (2013) and Lu and Qin (2014) for rainfall spatial correlation structure and statistical downscaling studies. Table 1 summarises key aspects of the data used in this study.

3 Methodology and Analysis Tools

As mentioned in the Introduction section, the aim of this study is to investigate the presence of scale-invariance in rainfall time series, and identify the corresponding scaling regimes. We approached this goal by first focusing on the properties of rainfall support in a monofractal framework, and then on rainfall intensity fluctuations in spectral and multifractal frameworks. In the following, we describe the analysis tools employed in this study.

3.1 Binary Series: Box-Counting Analysis

To understand rainfall support, we transformed the data into binary series (BS) by setting all values above a certain threshold to 1 and 0 otherwise (See Figure 2 for an illustration), and used box-counting analysis. The box-counting analysis involves dividing the BS into non-overlapping contiguous boxes of length τ and counting the number of boxes $N(\tau)$ registering rain (e.g., Mandelbrot, 1983; Falconer, 2004). The rainfall support is said to be scale-invariant if $N(\tau)$ displays power-law behavior of the form

$$N(\tau) \sim \tau^{-D_f} \tag{1}$$

The fractal dimension D_f is a measure of irregularity by which the rainfall support is distributed in the space it is embedded in. For rainfall binary time series, D_f lies between 0 and 1. D_f is part of a collection of dimensions called Renyi dimensions D_q. When $q = 0$, D_q is equal to aforementioned fractal dimension (or box counting dimension). When q = 1,2 the corresponding D_1 and D_2 are known as information and correlation dimensions respectively (e.g., Renyi, 1970; Gan et al, 2002). The correlation dimension D_2 has been employed by many studies to study dimensionality of chaotic systems (e.g., Islam et al, 1993; Gan et al, 2002, 2007). In this study we limit our focus to D_f and use it to characterize rain–no-rain intermittency in the rainfall BS. The fractal dimension is an effective tool to study the scaling properties of rainfall support but the amplitude variations in the rainfall signal are ignored. Therefore, we also estimated D_f of rainfall BS for different intensity thresholds.

It should be noted that in some studies box-counting analysis was used on the original rainfall series instead of binary series (e.g., Rubalcaba, 1997; Breslin and

Belward, 1999). The approach is similar to that described above except that it involves counting the number of boxes of varying size that would cover the time series plot (time on x-axis and rainfall intensity on y-axis). Since we analyze rainfall intensity fluctuations later in detail using spectral and multifractal analyses, we limit box-counting to the rainfall binary series. We would first focus on the rainfall support, characterize the fractal behavior, and gradually proceed to higher order analysis (power spectrum and multifractals).

3.2 Power Spectrum

The power spectrum is one of the basic tools to investigate the presence of scale-invariance in rainfall (e.g., Fraedrich and Larnder, 1993; Georgakakos et al, 1994; Verrier et al, 2011; Rysman et al, 2013; Mascaro et al, 2014). We obtained the power spectrum by applying discrete Fourier transform (DFT) on time series. The rainfall fluctuations are scale-invariant if the spectrum $E(f)$ displays power-law behavior of the form

$$E(f) \sim f^{-\beta} \tag{2}$$

where β is the slope of the spectrum in the double logarithmic domain (e.g., Fraedrich and Larnder, 1993), which is estimated using linear regression in logarithmic space. However, to reduce the effect of noise in the DFT spectra and to avoid excess weighting on higher frequencies, we pooled the DFT spectrum into logarithmic bins and estimated β for the log-binned spectrum. The log-log linearity was checked based on the R^2 value in regression. In this study, we estimated power spectrum for the rainfall full series (FS) and the corresponding BS thus obtaining spectral slopes β_{FS} and β_{BS} respectively.

The spectral slope β quantifies relative contribution of different frequency components to the overall variability of the time series. For example, the spectral slope of zero means equal contribution of all frequencies to the overall variability, as in the case of white noise. On the contrary, steeper power spectrum (or narrow spectral distribution) indicates that the contribution of low frequencies to the overall variability is higher compared to high frequencies. Therefore, steeper power spectrum is a characteristic of slowly varying time series (i.e. slower decay of autocorrelation with time) with a higher level of organization (e.g., Purdy et al, 2001; Rysman et al, 2013). Purdy et al (2001) further associated steeper spectrum to the existence of organized convective structures and flatter spectrum to the less organized stratiform rainfall. Since then, many studies have related spectral slopes to the presence of convective and stratiform structures in respective scaling regimes (e.g., Nykanen and Harris, 2003; Nykanen, 2008; Mascaro et al, 2013, 2014).

3.3 Multifractal Analysis

The analysis tools discussed to this point are based on zeroth- to second-order statistics, and provide only partial description of the process. Moreover, it has been shown that the fractal dimension of rainfall varies with the threshold used to define the support (e.g., Lovejoy et al, 1987). To better characterize such complex structure of rainfall, studies proposed analysis tools and models based on a more unified multifractal formalism (e.g., Schertzer and Lovejoy, 1987; Over and Gupta, 1996; Deidda et al, 1999; Venugopal et al, 2006). In this study, we used codimension based formalism and the corresponding moment scaling analysis (e.g.,

Schertzer and Lovejoy, 1987; Tessier et al, 1993) to characterize the multifractality in rainfall series.

3.3.1 Co-dimension Formalism and Moment Scaling Analysis

In co-dimension based multifractal formalism, the rain–no-rain threshold is defined as λ^{γ}, where $\lambda = T/\tau$ is the scale ratio for a given scale τ and outer scale T, and γ is referred to as the order of singularity. For a multifractal field Φ, the exceedance probabilities for different scales and singularities scale as

$$Pr(\Phi_{\lambda} > \lambda^{\gamma}) \sim \lambda^{-c(\gamma)} \tag{3}$$

where $c(\gamma)$ is the convex shaped fractal co-dimension function of γ (for details, see Lovejoy and Schertzer, 2007). It has been shown that fields with multifractal characteristics can be generated using multiplicative cascades, where large scale structures feed small scale structures (e.g., Schertzer and Lovejoy, 1987). Therefore, one way to characterize multifractality of a process is to reconstruct the multiplicative cascade and carry out moment scaling analysis. In moment scaling analysis, the rainfall fluctuations $\phi(t) = |R(t) - R(t-1)|$ are averaged over a range of scales τ (scale ratios λ) to obtain ϕ_{λ}. The statistical moments of various moment orders q are then estimated as $\langle \phi_{\lambda}^{q} \rangle$, where $\langle \cdot \rangle$ represents ensemble average. The rainfall fluctuations are multifractal if the statistical moments display power-law behavior with λ as follows

$$\langle \phi_{\lambda}^{q} \rangle \sim \lambda^{K(q)} \tag{4}$$

where $K(q)$ is a convex function of q (e.g., Lovejoy and Schertzer, 2007). To be consistent with box-counting analysis described in section 3.1, we write equation

4 in terms of τ instead of scale ratio λ as follows.

$$\langle \phi_\tau^q \rangle \sim \tau^{-K(q)} \tag{5}$$

3.3.2 'Universal' Multifractal Model

Theoretically, infinite number of parameters are required to characterize the $K(q)$ function. However, Schertzer and Lovejoy (1987) proposed a 'universal' multifractal model based on continuous-in-scale multiplicative cascades and Log-Levy stochastic generators, where the $K(q)$ function can be modeled as

$$K(q) = \begin{cases} \frac{C_1}{\alpha-1}(q^\alpha - q), & \text{if } 0 \leq \alpha < 1 \text{ or } 1 < \alpha \leq 2 \\ C_1 q log(q), & \text{if } \alpha = 1 \end{cases} \tag{6}$$

The parameter $C_1 \in [0, D]$ (D is the dimension of the embedding space) is the co-dimension of the mean of the process such that $c(C_1) = C_1 = K'(1)$. In other words, C_1 characterizes the degree of intermittency associated with the mean of the process. Higher the C_1 more intermittent and singular is the process. The parameter $\alpha \in [0, 2]$ is the Levy (or multifractality) index that describes the probability distribution of the underlying cascade generator. While $\alpha = 0$ corresponds to monofractal model, $0 < \alpha < 2$ ($\alpha \neq 1$) indicates log-Levy multifractals. The multifractal process is log-Cauchy when $\alpha = 1$ and lognormal when $\alpha = 2$ (e.g., Schertzer and Lovejoy, 1987, 1997). The parameters C_1 and α can be estimated using the double trace moments (DTM) technique (e.g., Tessier et al, 1993), in which the fluctuation field ϕ is (i) $\eta-$powered at the highest resolution, (ii) averaged to various temporal scales τ, and (iii) statistical moments of various orders q are estimated. The statistical moments of $\eta-$powered fields are referred to as

241 double trace moments, which scale with τ as

$$\langle (\phi^{\eta})_{\tau}^{q} \rangle \sim \tau^{-K(q,\eta)}, \qquad \text{where } K(q,\eta) = \eta^{\alpha} \cdot K(q) \tag{7}$$

242 Hence, α is the slope of $K(q,\eta)$ versus η in a double logarithmic plot for a fixed
243 q. The value of C_1 can be then obtained from equation 6.

244 4 Results and Discussion

245 As described in section 2, we have 31 years of hourly data from 49 gauges and 3
246 years of 1-minute data from five gauges. We analyzed both hourly and 1-minute
247 data using the tools described in the previous section, and investigated the presence
248 of scale-invariance. The following sections describe the scaling regimes in rainfall
249 support and intensity fluctuations, and the corresponding scaling exponents.

250 4.1 Fractal Dimension

251 *4.1.1 Hourly Rainfall Series*

252 The hourly rain gauge series was converted into binary series by setting all non-
253 zero values to 1 and 0 otherwise. Note that the minimum non-zero value in the
254 hourly data is 0.1 mm h^{-1}. The box-counting technique described in section 3.1
255 was then applied on the binary series. First, we counted the number of 1-h boxes
256 containing rain. We then increased the box size τ logarithmically (base 1.5 and
257 rounded off to the nearest integer value; τ therefore varied as 1,2,3,5,8,...,37877 h)
258 and counted the number of rain-boxes $N(\tau)$ for each τ. We repeated the analysis
259 for each of the 49 hourly rain gauge series and obtained 49 sequences of $N(\tau)$.
260 Figure 3 shows the minimum, median and maximum values of $N(\tau)$ as a function

of τ. Two clearly defined regimes of scale-invariance (linear variation in double-logarithmic plot) in $N(\tau)$ can be noticed in Figure 3: a regime spanning from 1 h to 38 h ($\sim$ 1.5 days) and a second regime from 195 h ($\sim$ 8 days) to 4 years. The two regimes are separated by a transition zone spanning from 1.5 - 8 days. Note that the scale breaks were identified using an iterative procedure.

The median values of $N(\tau)$ in the above two scaling regimes were fitted with a power law (equation 1) using linear regression in a double-logarithmic space. The corresponding slopes for the two scaling regimes are -0.38 and -1.0 respectively. Therefore, the rainfall support for the hourly data exhibits fractal structure with a fractal dimension $D_f = 0.38$ for τ ranging from 1 h to about 1.5 days. The D_f value of 1.0 for τ exceeding 8 days indicates that in this regime hourly rainfall occurrences are homogeneously distributed in time. In other words, every box of size $\tau > 8$ days always records a rain occurrence at some point. This so-called saturation of the rainfall process towards larger τ values has been reported in several studies (e.g., Olsson et al, 1992, 1993; Schmitt et al, 1998; Sivakumar, 2000b; Ghanmi et al, 2013). In addition to the median values of $N(\tau)$, we also fitted power laws to $N(\tau)$ sequence from each rain gauge and obtained corresponding D_f. We did not find considerable intergauge variability in D_f values (e.g. first row in Table 2).

To further understand the structure of rainfall support, we repeated above analysis for different thresholds of 0.1, 0.25, 0.5, 1, 2, 4, 8, and 10 mm h^{-1}. The inset in Figure 3 shows the variation of D_f with threshold. In Table 2, we list the D_f values and corresponding scaling regimes for all the thresholds considered in this study. Consistent with previous studies, the D_f value decreases with the increase in threshold. As the threshold increases from 0 mm h^{-1} to 10 mm h^{-1}, the corresponding rainfall occurrences are more sparsely distributed in time, which is

reflected in the rapid decrease in the value of D_f from 0.38 to 0.08. While the first scaling regime of 1 - 38 h is the same for all thresholds, the length of the saturation regime changes with threshold. For the threshold of 0 mm h^{-1}, the saturation regime starts at 195 h ($\sim$ 8 days). As the rainfall occurrences get sparser with the increase of threshold, it requires a larger box size to reach saturation. Therefore, the saturation regime starts at 292 h ($\sim$ 12 days) for thresholds between 0.1 and 2 mm h^{-1}, and at 438 h ($\sim$ 18 days) for thresholds of 4 mm h^{-1} and 10 mm h^{-1} (Table 2). The rapid variation of D_f with threshold clearly indicates that a multifractal framework is more suitable than a simple monofractal approach to characterize the variability in rainfall time series.

4.1.2 1-minute Rainfall Series

The box-counting analysis was then applied on 1-minute rainfall series for a threshold of 0 mm min^{-1} and for τ varying logarithmically from 1 to 287627 min ($\sim$ 200 days). Note that unlike hourly data, the box-counting analysis of 1-minute rainfall series was limited to only a single threshold of 0 mm min^{-1}. Figure 4 shows minimum, median and maximum values of $N(\tau)$ as a function of τ. Three well-defined scaling regimes were observed (Figure 4): i) regime 1 extending from 1 to 86 minutes with a $D_f = 0.56$, ii) regime 2 from 86 to 1478 minutes ($\sim$ 1 day) with a $D_f = 0.37$, and iii) a saturation regime starting from 11223 minute ($\sim$ 7.8 days). Regimes 2 and 3 are separated by a transition regime. In general, the results from the 1-minute rainfall analysis agree well with the hourly rainfall analysis presented in the previous section. The 86 min - 1 day regime (D_f of 0.37) in 1-minute analysis is similar to 1 h - 1.5 days regime (D_f of 0.38) of hourly data analysis. Similarly, the saturation regime starts at 7.8 days in the 1-minute data

analysis, while it starts at 8 days in hourly results. The slight differences in regime breaks in hourly and 1-minute analyses are mainly due to different τ increments used for these two datasets.

We attempt to relate the observed scaling behavior to the duration of rain events and dry periods extracted using 1-minute resolution data (3 years of data at five stations). Note that in this analysis, a gap of more than 10 minutes is considered as a dry period. In other words, if two non-zero sequences are separated by a gap $\leq$ 10 minute then they are considered as a single event.

On average, 2276 rain events were recorded in three years starting from July 2010 to June 2013 (Table 3). The average duration of a rain event is $\sim$ 18 minutes and the maximum duration varies from 371 – 822 minutes among five stations. However, only 4 % of rain events are of duration longer than 90 minutes. Therefore, the scaling regime of 1 – 86 minutes observed in Figure 4 mainly reflects variability within the events, and the scaling regime of 86 minutes to 1 day is more likely to contain more than one event and mainly reflects inter-event variability. The relatively high D_f in 1 – 86 min regime compared to 86 min - 1 day regime (Figure 4) suggests denser structure in the former regime with rainy minutes closely clustered together. In other words, 1 – 86 minutes regime contains several smaller scale densely arranged rainy boxes that decrease rapidly with the increase in box size, whereas 86 minutes – 1 day regime is mainly characterized by rainy boxes that are sparsely distributed in time. The average duration of dry period is $\sim$ 11.3 h and the maximum duration varies from 290 – 419 h among five stations (Table 3). However, only 0.3 % of dry periods are of duration longer than 8 days (192 h). Therefore it can be said that the average dry period duration lies closer to the end

of fractal regime and the maximum duration dry period is closer to the beginning of saturation regime.

4.1.3 Comparison with Previous Studies

Olsson et al (1992) and Olsson et al (1993) also reported average dry period duration lying closer to the end of the fractal regime. Similarly, Ghanmi et al (2013) noted that the beginning of the saturation period at 113 days in their study is due to the 4-month dry period typical of their study region. The two-regime pattern observed in hourly data analysis is similar to that shown by Sivakumar (2000b) for six-hourly data. However, they did not report D_f values and the regime breaks, which limits the comparison. Gebremichael et al (2007) also reported a two-regime pattern in their fractal analysis of hourly rainfall data collected during one North American monsoon season in Mexico. Their results show a fractal regime ranging from 2 to 16 h and the saturation regime starting at 2.7 days.

The three-regime pattern observed in 1-minute data analysis is similar to that showed by Olsson et al (1992, 1993) for 1-minute rainfall data in Lund, Sweden. They reported that the first regime extends from 1 - 45 minutes with a D_f value of 0.82. The smaller D_f of 0.56 in the current study for a similar sub-hourly scaling regime of 1 - 86 minutes suggests that rainy minutes at event scales are sparser in Singapore than Lund, Sweden. The D_f value of 0.37 observed for scales of 86 minutes - 1 day is same as the one reported by Olsson et al (1992, 1993), although the scale range extended up to 1 week in the latter.

Schmitt et al (1998) observed a two-regime pattern in box-counting analysis of 28 years of 10-minute rainfall data from Uccle, Belgium. The study reported a scaling regime from 10 min to 3.5 days with a D_f of 0.55 followed by a satura-

tion regime. Ghanmi et al (2013) analyzed 5-minute rainfall data from a semi-arid mediterranean region in Tunisia and reported scaling regime extending from 5 minute to 2 days with a D_f of 0.44 followed by a transition regime and a saturation regime starting at 113 days. The overall scaling behavior of N(τ) vs τ (i.e. scale breaks and the D_fs) in these studies are different from the three-regime pattern observed in our study. The disagreement could be attributed to different climates the data were recorded, and different data characteristics (resolutions, record lengths, quantization etc.). A rigorous comparison of D_f values and corresponding scaling regimes from the current study with those reported in the literature, taking into account the differences in data resolutions, record lengths, thresholds, and geographical locations is beyond the scope of this study.

4.2 Power Spectrum

We estimated power spectrum of rainfall full series (FS) and the corresponding binary series (BS) using discrete Fourier transforms. The threshold applied to obtain the binary series is 0 mm h^{-1} for hourly data and 0 mm min^{-1} for 1-minute data.

4.2.1 Hourly Rainfall Series

The spectrum from each gauge series was averaged into logarithmic bins to reduce noise and to avoid excess weighting on higher frequencies during linear regression. Figure 5 shows the minimum, median, and the maximum values (i.e. the intergauge variability) of log-binned spectrum. Two distinct scaling regimes can be seen in

the FS power spectrum: regime 1 from 2 h to 28 h with a β_{FS} of 0.46 and regime 2 from 28 h to 1.5 months with a β_{FS} of 0.15 (Figure 5).

As discussed in section 3.2, the spectral slope β characterizes the degree of smoothness or organization in the time series. Higher β_{FS} in regime 1 indicates that the variability in this regime is predominantly due to low frequency components. As the time period increases beyond 28 h (i.e. regime 2), the spectrum is flatter suggesting greater interaction among all frequency components in this regime. In other words, the autocorrelation function decays slowly in regime 1 compared to regime 2. Therefore, regime 1 is characterized by smoother and organized structures compared to regime 2. The noisy spectrum beyond 1.5 months with a slope close to zero is a combined effect of limited sample size and large-scale (seasonal to climatic) fluctuations. The BS spectrum displayed the same two-regime pattern as the FS spectrum, although with higher spectral slopes (Figure 5). Higher β_{BS} values suggest more organization in BS than the actual rainfall series.

4.2.2 1-minute Rainfall Series

To better understand the high-frequency component of rainfall variability, we repeated spectral analysis for 1-minute rainfall data available at five stations. Figure 6 shows the minimum, median and the maximum values of the log-binned spectrum. The spectra of 1-minute rainfall FS and BS displayed three scaling regimes: regime 1 from 4 minutes to 2 h, regime 2 from 2 h to 1 day, and regime 3 from 1 day to 1 month (Figure 6). The high frequency end of the spectrum (regime 1) has the highest β_{FS} value of 1.5 followed by a β_{FS} of 0.49 and 0.12 in regimes 2 and 3 respectively. In the high frequency regime (regime 1), the spectrum of binary series is very sensitive to energy leaks, as also observed by Molini et al (2009). This

could be the reason behind the curved pattern in the binary spectrum at very high frequencies, and also partially explains why the BS spectrum is not steeper than the FS spectrum in this regime. The scaling regimes 2 and 3 are similar to regimes 1 and 2 observed in hourly spectral analysis (Figures 5 and 6).

By taking a unified look at hourly and 1-minute spectra, it can be said that the regime 1 (4 minutes to 2 h), which has the highest β_{FS} of 1.5 is characterized by the presence of smooth and organized structures typical of convective systems. This regime represents variability within the storms as discussed in section 4.1.2. As the time period increases beyond 2 h (i.e. regime 2), the spectrum is flatter compared to regime 1 indicating that the variability in this regime decreases slowly with time scale, which is typical of mesoscale systems. As discussed in section 4.1.2, this regime represents inter-event variability. Beyond the time scale of 1 day (i.e. regime 3), the spectral slope is very low indicating that a large number of frequency components contribute to the overall variability resulting in a broad spectral distribution.

4.2.3 Comparison with Previous Studies

The general pattern of the spectral scaling regimes observed in this study is consistent with previous studies (e.g., Fraedrich and Larnder, 1993; Georgakakos et al, 1994; Kiely and Ivanova, 1999; Verrier et al, 2011; Mascaro et al, 2013). The scaling regime of 2 h - 1 day with β_{FS} of 0.49 is comparable to the scaling regime of 2.4 h - 3 days with a β of 0.5 reported by Fraedrich and Larnder (1993), 2 h - 1 day with a β of 0.52 reported by Kiely and Ivanova (1999), 3 h - 3 days with a β of 0.41 reported by Verrier et al (2011), and 2.4 h - 3 days with a β of 0.55 reported by Mascaro et al (2013). At higher frequencies, the scaling regime of 4 minutes

427 - 2 h is comparable to that observed in recent studies employing high-resolution
428 rainfall data (Verrier et al, 2011; Mascaro et al, 2013, 2014). In general it can be
429 said that the spectral slopes vary from 1.1 to 1.6 at higher frequencies (seconds to
430 2-3 hours), 0.4 to 0.7 for medium frequencies (2-3 hours to 2-3 days), and 0.1 to
431 0.3 for time scales longer than three days. The spectral slopes for BS are higher
432 compared to FS in all regimes, which is consistent with previous studies (e.g.,
433 Molini et al, 2009; Mascaro et al, 2013).

434 ## 4.3 Multifractal Analysis

435 ### *4.3.1 Hourly Rainfall Series*

436 Following the approach described in section 3.3.1, the first-order hourly rainfall
437 fluctuations at the highest resolution are gradually averaged to coarser resolutions
438 (τ) and various moments of order q are estimated. It should be noted that we
439 considered complete series including zeros in moment scaling analysis. Unlike box-
440 counting analysis where τ is varied logarithmically in steps of 1.5 (please refer
441 to section 4.1.1), τ in this section is varied according to steps of factor 2. In
442 Figure 7, we plot the trace moments ($\langle \phi_\lambda^q \rangle$) against τ. As in previous sections, the
443 vertical bars in Figure 7 indicate intergauge variability, and the scaling regimes
444 were identified based on an iterative procedure. The trace moments were found
445 to be scale-invariant for the τ ranging from 1 h to 5 days. The median values of
446 trace moments were then fitted with power-laws and the corresponding scaling
447 exponents ($k(q)_{med}$) were obtained. The nonlinear variation of the slopes $k(q)_{med}$
448 (filled circles in Figure 8) with moment order q indicates multiscaling behavior in
449 rainfall fluctuations.

We modeled the behavior of $k(q)_{med}$ using the universal multifractal (UM) model (section 3.3.2) and estimated parameters C_1 and α using the DTM technique described in section 3.3.2. The thick line in Figure 8 shows the UM model fitted to $k(q)_{med}$ values. The values of C_1 and α for the median scenario are 0.61 and 0.36 respectively. Figure 8 also shows UM models fitted to the $k(q)$ obtained from each gauge series, and the corresponding values of C_1 and α ranged from 0.58 to 0.62, and 0.34 to 0.39 respectively. There is a systematic deviation between empirical $k(q)$ and the fitted UM model at lower moment orders. As mentioned in section 3.3.2, $k(0)$ is related to the codimension of the support, and characterizes the on-off intermittency (e.g., Lovejoy et al, 2008). According to the universal multifractal model shown in equation 6, $k(0) = 0$ or the signal is nonzero for all the scales. In reality, the rainfall data consists of zeros, which are partly due to the minimum detectable threshold of the measuring device and partly due to the natural duality of the rainfall process. The influence of zero-rainfall values on the estimated universal multifractal parameters has been a subject of recent research (De Montera et al, 2009; Verrier et al, 2011), which showed that the presence of zeros in the data would result in biased estimates of C_1 and α. Therefore, we note that the values of the C_1 and α obtained in this study must be taken with caution. Nevertheless, the behavior of $k(q)$ function suggests that the rainfall fluctuations for this region display multiscaling behavior.

4.3.2 1-minute Rainfall Series

To understand multiscaling behavior at high resolutions, we extended the moment scaling analysis to 1-minute resolution rainfall observations. Since the percentage of zeros in 1-minute rainfall observations is very high (See Table 1), and because the

zero values severely affect the moment scaling analysis (as discussed in previous section), we limited this section to individual events. From the high-resolution data, we extracted events that are at least 64 min long. A total of 111 events were extracted from the data at five stations, and moment scaling analysis was carried out. Figure 9 shows the trace moments as a function of averaging scale τ. A scaling regime spanning from 1 minute to 64 minutes can be seen from Figure 9. The median values of trace moments were then fitted with power-laws and the corresponding scaling exponents ($k(q)_{med}$) were obtained. The variation of $k(q)_{med}$ was then parameterized using the UM model. Figure 10 shows the variation of empirical $k(q)_{med}$, and the fitted UM model. The values of C_1 and α for the median scenario are 0.11 and 1.10 respectively. We also fitted UM model to the $k(q)$ values of each event. Large variability can be seen in the UM models fitted to rainfall events (Figure 10). The values of C_1 and α ranged from 0.06 to 0.18, and 0.59 to 1.74 respectively. However, 90% of events have C_1 and α in the range of 0.07 to 0.16, and 0.79 to 1.38 respectively.

5 Concluding Remarks

Temporal structure of rainfall in the Maritime Continent, particularly towards higher resolutions is poorly understood. To fill this gap, we analyzed a long record of hourly and 1-minute resolution rainfall data from a dense gauge network in Singapore and characterized temporal scale-invariance in rainfall. Specifically, we used box-counting analysis to study zero-rainfall intermittency, and spectral and moment scaling analyses to study intensity fluctuations.

The study showed that the rainfall support displays fractal behavior but within a limited range of scales starting from 1 minute to 1.5 h, and 1.5 h to 1 day. The corresponding fractal dimensions are 0.56 and 0.37 respectively. It was also found that the fractal dimension varies as a decreasing function of the threshold used to define the binary series. The study then made an attempt to relate the scaling regimes to event and dry period durations. The fractal regimes mentioned above roughly characterize intra- and inter-event variability. The higher fractal dimension for smaller scales suggests densely arranged and evenly distributed rainy intervals compared to inter-event scales. In addition, results showed that the saturation regime begins at approximately 8 days. In other words, every time window of size > 8 days always records a rain occurrence at some point. It was also observed that the end of fractal regime and the beginning of saturation regime are related to the dry period characteristics.

The spectral analysis of rainfall series showed three distinct scaling regimes of 4 minutes to 2h, 2 h to 24 h, and 24 h to 1 month with spectral exponents of 1.5, 0.49, and 0.12 respectively. The steeper spectrum in the 4 minute - 2 h regime indicates the presence of smooth and organized convective structures, whereas the flatter spectrum in the 2 h - 24 h regime suggests the presence of larger scale systems. The power spectrum of binary series also showed similar three regime pattern but the spectral exponents were found to be 1.5, 0.77, and 0.27 respectively. The moment scaling analysis confirmed the presence of multiscaling behavior in rainfall fluctuations for scales ranging from 1 h – 5 days. The corresponding $k(q)$ vs q pattern was parameterized using the Universal Multifractal model, and the multifractality index α and the intermittency parameter C_1 were found to be 0.36 and 0.61 respectively. The study also extended moment scaling analysis to high-

resolution data of 111 individual rainfall events, which are at least 64 minutes long. The trace moments displayed scaling behavior in the range of 1 – 64 minutes, and the corresponding α and C_1 values for event scale were found to be 1.10 and 0.11 respectively

A challenging task is to relate observed scaling behavior to the physical mechanisms behind Singapore rainfall. A step forward in that direction would be to categorize rainfall series according to southwest, northeast and intermonsoon seasons, and estimate scaling exponents. This would provide insights into the effect of various rainfall mechanisms such as intense convective storms, monsoon surges and squall lines on the scale-invariance behavior of rainfall. However, such an exercise should be carried out using high-resolution time series. The three-year record of 1-minute resolution rainfall available for this study is not long enough for such an analysis.

In general, the scaling regimes observed in this study were found to be consistent with those reported in previous studies although the numerical values of scaling exponents were slightly different. The results from this study would not only improve our understanding of the rainfall structure in Singapore and the surrounding equatorial region, but they also help us in building and parameterizing parsimonious models and statistical downscaling techniques for the tropical rainfall.

Acknowledgements This study was supported by Singapores Ministry of Education (MOM) AcRF Tier 2 (M4020182.030) project. The authors appreciate the support from National Environmental Agency of Singapore for providing rain gauge data.

References

Breslin M, Belward J (1999) Fractal dimensions for rainfall time series. Math Comput Simulat 48(4):437–446

Chatterjea K (1998) The impact of tropical rainstorms on sediment and runoff generation from bare and grasscovered surfaces: a plot study from singapore. Land Degrad Dev 9(2):143–157

Chatterjea K (2011) Severe wet spells and vulnerability of urban slopes: case of singapore. Natural Hazards 56(1):1–18

Chia LS, Foong FS (1991) Climate and weather. In: Tay DBH, Chia LS, Rahman A (eds) The Biophysical Environment of Singapore, National University of Singapore Press, pp 13–49

De Montera L, Barthès L, Mallet C, Golé P (2009) The effect of rain–no rain intermittency on the estimation of the universal multifractals model parameters. J Hydrometeorol 10(2):493–506

Deidda R, Benzi R, Siccardi F (1999) Multifractal modeling of anomalous scaling laws in rainfall. Water Resour Res 35(6):1853–1867

Deidda R, Badas M, Piga E (2004) Space-time scaling in high intensity Tropical Ocean Global Atmosphere Coupled Ocean-Atmosphere response Experiment TOGA-COARE storms. Water Resour Res 40(2):W02,506

Falconer K (2004) Fractal geometry: mathematical foundations and applications. Wiley

Fong M (2012) The weather and climate of Singapore. Meteorological Service Singapore, Singapore

567 Fraedrich K, Larnder C (1993) Scaling regimes of composite rainfall time series.
568 Tellus 45(4):289–298
569 Gan TY, Wang Q, Seneka M (2002) Correlation dimensions of climate subsystems
570 and their geographic variability. J Geophys Res 107(D23):ACL23–1–ACL23–17
571 Gan TY, Gobena AK, Wang Q (2007) Precipitation of southwestern canada:
572 Wavelet, scaling, multifractal analysis, and teleconnection to climate anoma-
573 lies. J Geophys Res 112(D10):D10,110
574 Gaume E, Mouhous N, Andrieu H (2007) Rainfall stochastic disaggregation mod-
575 els: Calibration and validation of a multiplicative cascade model. Adv Water
576 Res 30(5):1301–1319
577 Gebremichael M, Vivoni ER, Watts CJ, Rodríguez JC (2007) Submesoscale spa-
578 tiotemporal variability of north american monsoon rainfall over complex terrain.
579 J Climate 20(9):1751–1773
580 Gebremichael M, Krajewski WF, Over T, Takayabu Y, Arkin P, Katayama M
581 (2008) Scaling of tropical rainfall as observed by TRMM precipitation radar.
582 Atmos Res 88(3-4):337–354
583 Georgakakos KP, Carsteanu A, Sturdevant-Rees P, Cramer J (1994) Observation
584 and analysis of midwestern rain rates. J Appl Meteorol 33(12):1433–1444
585 Ghanmi H, Bargaoui Z, Mallet C (2013) Investigation of the fractal dimension of
586 rainfall occurrence in a semi-arid mediterranean climate. Hydrol Sci J 58(3):483–
587 497
588 Islam S, Bras R, Rodriguez-Iturbe I (1993) A possible explanation for low corre-
589 lation dimension estimates for the atmosphere. J Appl Meteor 32(2):203–208
590 Kiely G, Ivanova K (1999) Multifractal analysis of hourly precipitation. Physics
591 and Chemistry of the Earth 24(7):781–786

592 Licznar P, Łomotowski J, Rupp DE (2011) Random cascade driven rainfall disag-
593 gregation for urban hydrology: An evaluation of six models and a new generator.
594 Atmos Res 99(3-4):563–578
595 Lovejoy S (1982) Area-perimeter relation for rain and cloud areas. Science
596 216(4542):185–187
597 Lovejoy S, Mandelbrot B (1985) Fractal properties of rain, and a fractal model.
598 Tellus 37(3):209–232
599 Lovejoy S, Schertzer D (2007) Scale, scaling and multifractals in geophysics:
600 Twenty years on. In: Tsonis A, Elsner J (eds) Nonlinear Dynamics in Geo-
601 sciences, Springer, New York, pp 311–337
602 Lovejoy S, Schertzer D, Tsonis A (1987) Functional box-counting and multiple
603 elliptical dimensions in rain. Science 235(4792):1036–1038
604 Lovejoy S, Schertzer D, Allaire V (2008) The remarkable wide range spatial scaling
605 of TRMM precipitation. Atmos Res 90(1):10–32
606 Lu Y, Qin XS (2014) Multisite rainfall downscaling and disaggregation in a tropical
607 urban area. J Hydrol 509:55–65
608 Mandapaka PV, Qin X (2013) Analysis and characterization of probability distri-
609 bution and small-scale spatial variability of rainfall in singapore using a dense
610 gauge network. J Appl Meteor Climatol 52(12):2781–2796
611 Mandapaka PV, Lewandowski PA, Eichinger WE, Krajewski WF (2009) Multi-
612 scaling analysis of high resolution space-time lidar-rainfall. Nonlinear Processes
613 in Geophysics 16(5):579–598
614 Mandapaka PV, Villarini G, Seo BC, Krajewski WF (2010) Effect of radar-rainfall
615 uncertainties on the spatial characterization of rainfall events. J Geophys Res
616 115(D17):D17,110, DOI 10.1029/2009JD013366

617 Mandelbrot BB (1983) The fractal geometry of nature. Times Books
618 Mascaro G, Deidda R, Hellies M (2013) On the nature of rainfall intermittency as
619 revealed by different metrics and sampling approaches. Hydrol Earth Syst Sci
620 17(1):355–369, DOI 10.5194/hess-17-355-2013
621 Mascaro G, Vivoni ER, Gochis DJ, Watts CJ, Rodriguez JC (2014) Temporal
622 downscaling and statistical analysis of rainfall across a topographic transect
623 in northwest mexico. J Appl Meteor 53(4):910–927, DOI 10.1175/JAMC-D-13-
624 0330.1
625 Molini A, Katul GG, Porporato A (2009) Revisiting rainfall clustering and inter-
626 mittency across different climatic regimes. Water Resour Res 45:W11,403
627 Nykanen D (2008) Linkages between orographic forcing and the scaling properties
628 of convective rainfall in mountainous regions. J Hydrometeorol 9(3):327–347
629 Nykanen D, Harris D (2003) Orographic influences on the multiscale statistical
630 properties of precipitation. J Geophys Res 108(D8):8381
631 Olsson J (1995) Limits and characteristics of the multifractal behavior of a high-
632 resolution rainfall time series. NPG 2(1):23–29
633 Olsson J, Niemczynowicz J, Berndtsson R, Larson M (1992) An analysis of the
634 rainfall time structure by box counting—some practical implications. J Hydrol
635 137(1):261–277
636 Olsson J, Niemczynowicz J, Berndtsson R (1993) Fractal analysis of high-
637 resolution rainfall time series. J Geophys Res 98(D12):23,265–23,274
638 Over T, Gupta V (1996) A space-time theory of mesoscale rainfall using random
639 cascades. J Geophys Res 101:26,319–26,331
640 Pathirana A, Herath S, Yamada T (2003) Estimating rainfall distributions at high
641 temporal resolutions using a multifractal model. Hydrol Earth Syst Sci 7:668–

679

Purdy J, Harris D, Austin G, Seed A, Gray W (2001) A case study of orographic rainfall processes incorporating multiscaling characterization techniques. J Geophys Res 106(D8):7837–7845

Renyi A (1970) Probability Theory. North-Holland, Amsterdam

Rubalcaba J (1997) Fractal analysis of climatic data: annual precipitation records in spain. Theor Appl Climatol 56(1-2):83–87

Rysman JF, Verrier S, Lemaître Y, Moreau E (2013) Space-time variability of the rainfall over the western mediterranean region: A statistical analysis. J Geophys Res Atmos pp n/a–n/a, DOI 10.1002/jgrd.50656

Schertzer D, Lovejoy S (1987) Physical modeling and analysis of rain and clouds by anisotropic scaling multiplicative processes. J Geophys Res 92(D8):9693–9714

Schertzer D, Lovejoy S (1997) Universal multifractals do exist!: Comments on "a statistical analysis of mesoscale rainfall as a random cascade". J Appl Meteorol 36(9):1296–1303

Schmitt F, Vannitsem S, Barbosa A (1998) Modeling of rainfall time series using twoäêstate renewal processes and multifractals. J Geophys Res 103(D18):23,181–23,193

Sivakumar B (2000a) Fractal analysis of rainfall observed in two different climatic regions. Hydrol Sci J 45(5):727–738

Sivakumar B (2000b) A preliminary investigation on the scaling behaviour of rainfall observed in two different climates. Hydrol Sci J 45(2):203–219

Svensson C, Olsson J, Berndtsson R (1996) Multifractal properties of daily rainfall in two different climates. Water Resour Res 32(8):2463–2472

666 Tessier Y, Lovejoy S, Schertzer D (1993) Universal multifractals: Theory and ob-
667 servations for rain and clouds. J Appl Meteorol 32(2):223–250
668 Venugopal V, Foufoula-Georgiou E, Sapozhnikov V (1999) Evidence of dynamic
669 scaling in space-time rainfall. J Geophys Res 104(D24):31,599–31,610
670 Venugopal V, Roux S, Foufoula-Georgiou E, Arneodo A (2006) Revisiting multi-
671 fractality of high-resolution temporal rainfall using a wavelet-based formalism.
672 Water Resour Res 42(6)
673 Verrier S, Mallet C, Barthès L (2011) Multiscaling properties of rain in the time do-
674 main, taking into account rain support biases. J Geophys Res 116(D20):D20,119,
675 DOI 10.1029/2011JD015719
676 Watts IEM (1955) Rainfall of Singapore island. Singapore J Trop Geo 7:1–71
677 Yonghe L, Kexin Z, Wanchang Z, Yuehong S, Hongqin P, Jinming F (2013) Multi-
678 fractal analysis of 1-min summer rainfall time series from a monsoonal watershed
679 in eastern china. Theor Appl Climatol 111(1-2):37–50, DOI 10.1007/s00704-012-
680 0627-9

Table 1 Summary of hourly and 1-minute data available for this study.

	Hourly Data	1-minute Data
Time Period	01/01/1980 - 31/12/2010	01/07/2010 - 30/06/2013
Number of gauges	49	5
% of zeros	92.54	98.66
Average rainfall	0.28 mm h^{-1}	0.005 mm min^{-1}
Maximum rainfall	130.7 mm h^{-1}	4.4 mm min^{-1}

Table 2 List of minimum, median and maximum (of 49 values) fractal dimensions and the corresponding scaling regimes observed in hourly data for different rain–no-rain thresholds.

Threshold	Regime 1				Saturation Regime			
mm h^{-1}	Min	Median	Max	Scale Range	Min	Median	Max	Scale Range
0.0	0.36	0.38	0.40	1 - 38 h	0.97	1.00	1.00	195 h onwards
0.1	0.34	0.35	0.38	1 - 38 h	0.97	1.00	1.00	292 h onwards
0.25	0.32	0.33	0.34	1 - 38 h	0.97	1.00	1.00	292 h onwards
0.5	0.28	0.29	0.30	1 - 38 h	0.97	1.00	1.00	292 h onwards
1.0	0.24	0.25	0.26	1 - 38 h	0.97	1.00	1.00	292 h onwards
2.0	0.19	0.20	0.21	1 - 38 h	0.97	1.00	1.00	292 h onwards
4.0	0.15	0.16	0.17	1 - 38 h	0.97	1.00	1.00	438 h onwards
10.0	0.08	0.08	0.09	1 - 38 h	0.96	0.99	1.00	438 h onwards

Table 3 Rainfall event and dry period statistics estimated using 1-minute data.

	s7	s8	s44	s89	s105
Number of events	2356	2441	2172	2051	2362
Average duration of events (min)	17.6	17.7	18.0	18.4	18.1
Maximum duration of events (min)	403	822	413	371	528
Average duration of dry period (h)	10.9	10.5	11.8	12.5	10.8
Maximum duration of dry period (h)	308.4	365.8	393.8	418.7	289.5

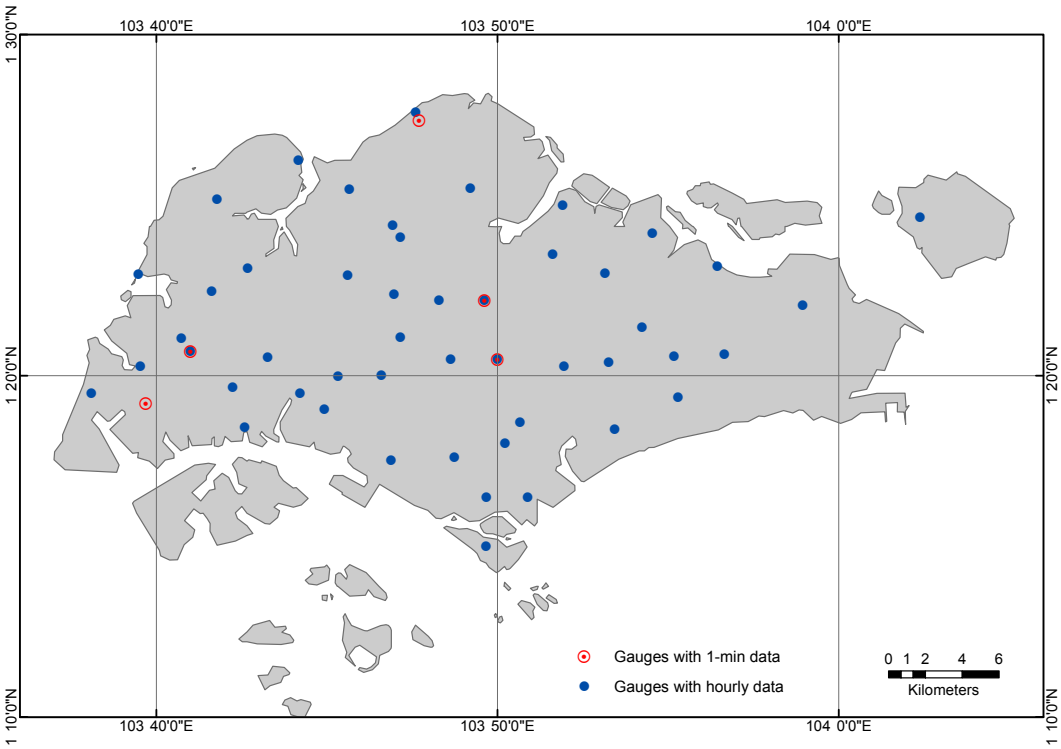

Fig. 1 Map of Singapore showing the location of rain gauges used in this study. There are 49 gauges with hourly and 5 gauges with 1-minute resolution rainfall data.

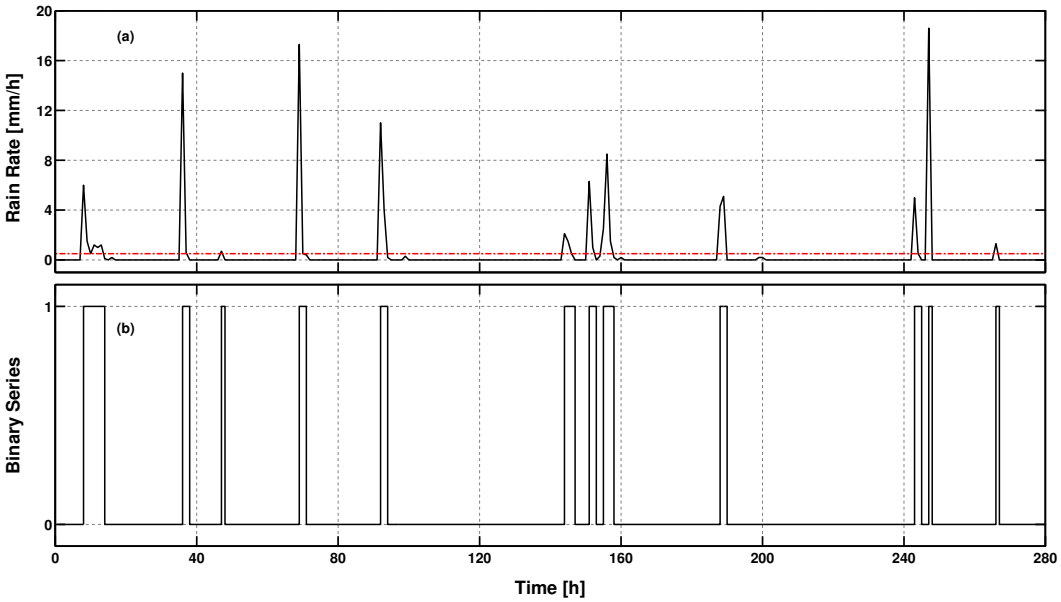

Fig. 2 An illustration of hourly rainfall time series and the corresponding binary series obtained with a threshold of 0.5 mm h^{-1}

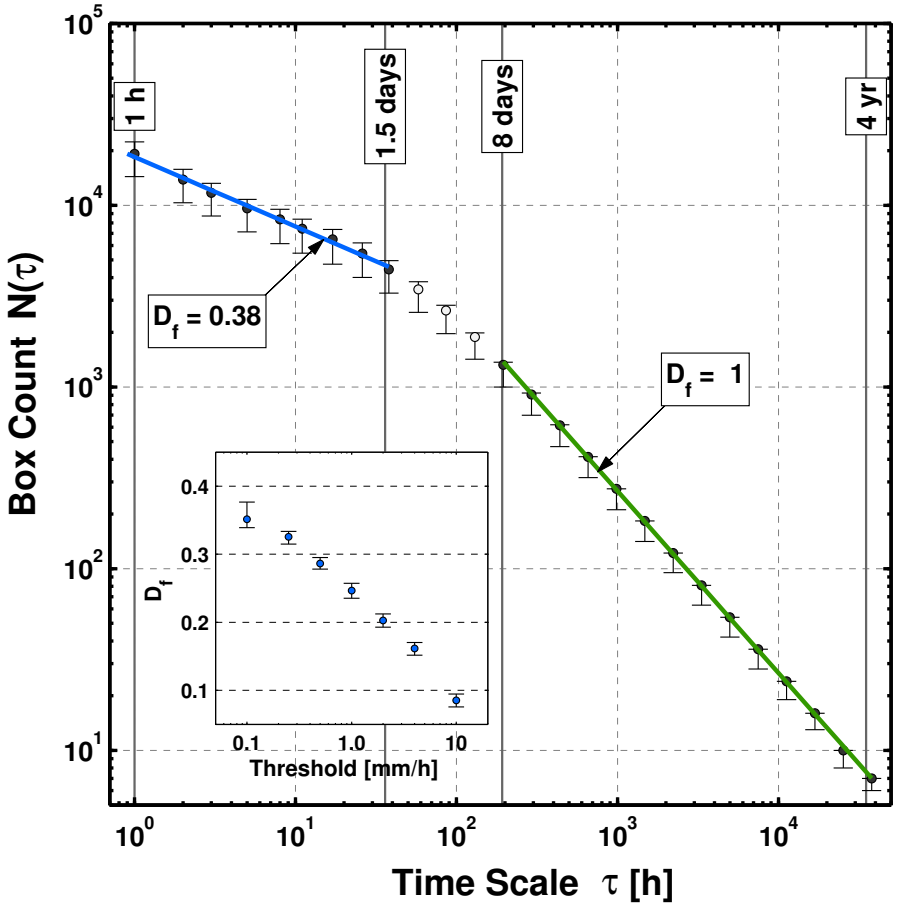

Fig. 3 Number of rainy boxes N(τ) as a function of time interval τ for the hourly binary series with a threshold of 0 mm h^{-1}. The circles represent median value (out of 49 values) of N(τ), and the vertical bars indicate intergauge variability. The Figure also shows the power laws (solid lines) fitted to the median values of N(τ) in the two scaling regimes (filled circles) and the corresponding fractal dimensions (D_f). The inset shows the variation of D_f with different zero-nonzero rainfall thresholds.

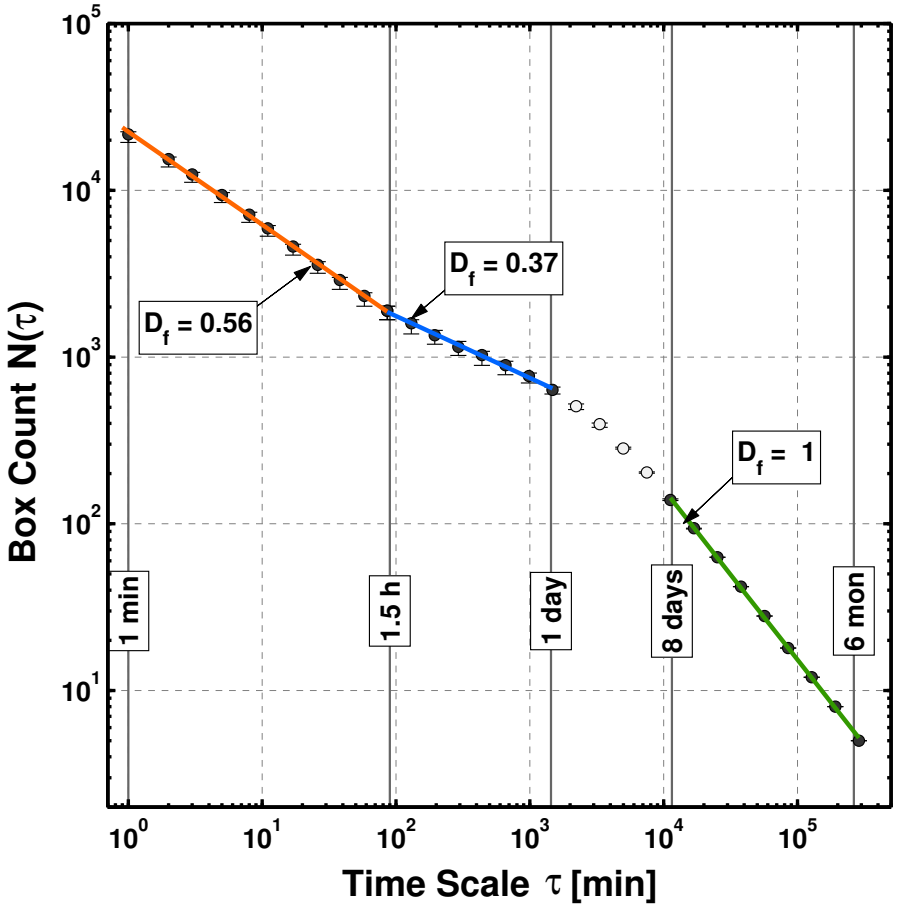

Fig. 4 Number of rainy boxes N(τ) as a function of time interval τ for the 1-minute binary series with a threshold of 0 mm min^{-1}. The circles represent median value (out of 5 values) of N(τ), and the vertical bars indicate intergauge variability. The Figure also shows the power laws (solid lines) fitted to the median values of N(τ) in the three scaling regimes (filled circles) and the corresponding fractal dimensions (D_f).

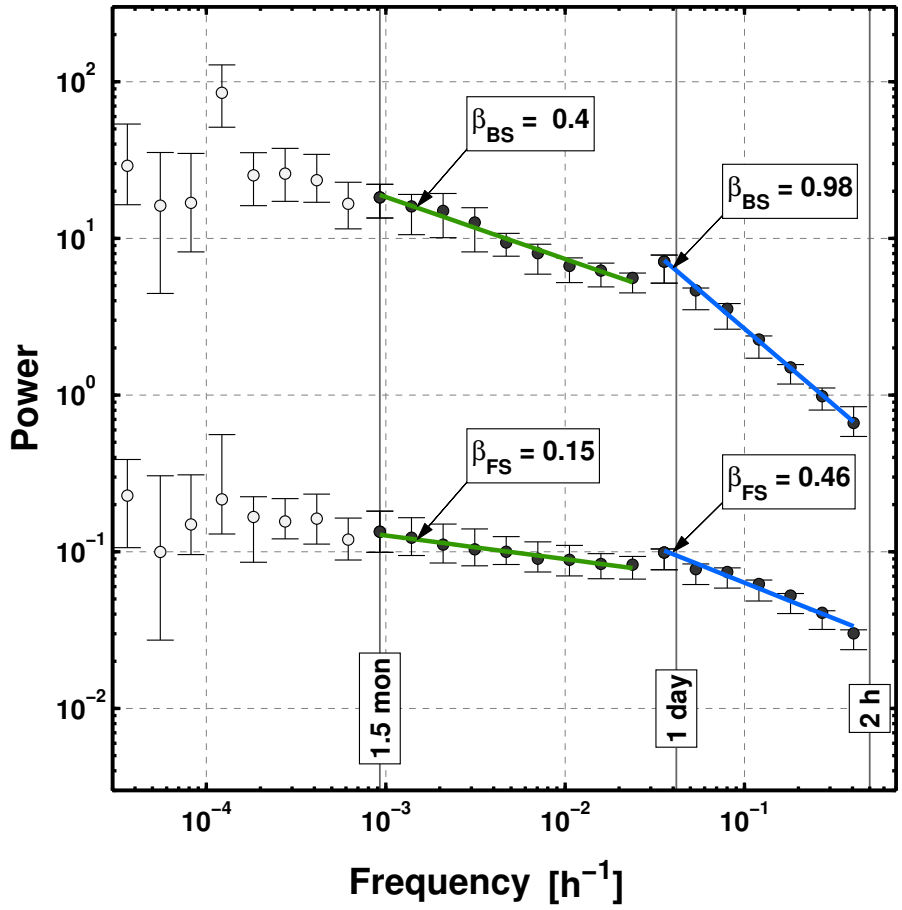

Fig. 5 Power spectrum of hourly rainfall full series (FS) and the corresponding binary series (BS). The circles represent median value (out of 49 values) of spectrum, and the vertical bars indicate intergauge variability. The solid lines represent power laws fitted in the respective scaling regimes.

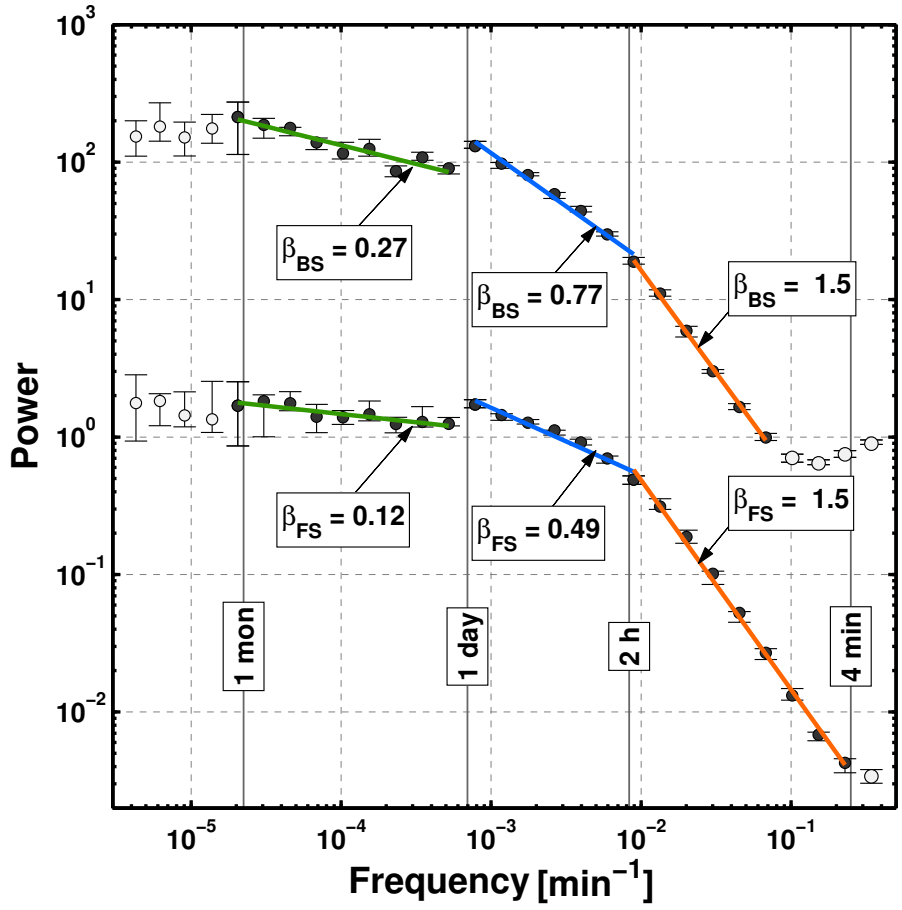

Fig. 6 Power spectrum of 1-minute rainfall full series (FS) and the corresponding binary series (BS). The circles represent median value (out of 5 values) of spectrum, and the vertical bars indicate intergauge variability. The solid lines represent power laws fitted in the respective scaling regimes.

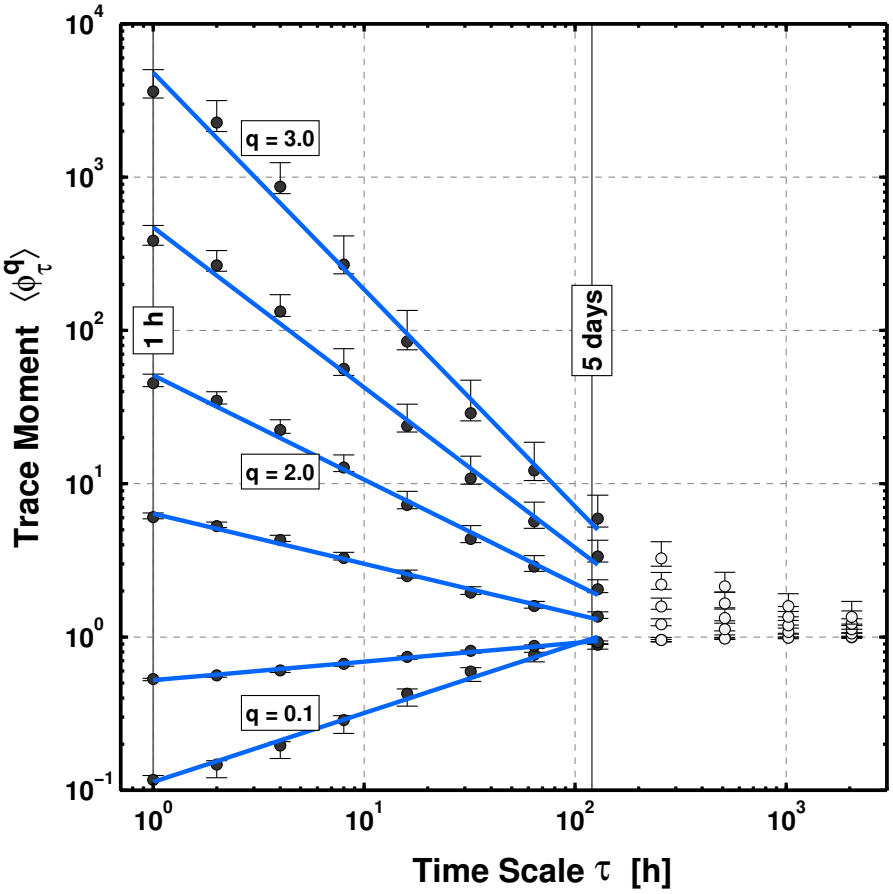

Fig. 7 Temporal scale-invariance in trace moments obtained from hourly data for different moment orders. The circles represent median value (out of 49 values) of spectrum, and the vertical bars indicate intergauge variability. The solid lines represent power laws fitted to the filled circles in the scaling regime of 1 h - 5 days.

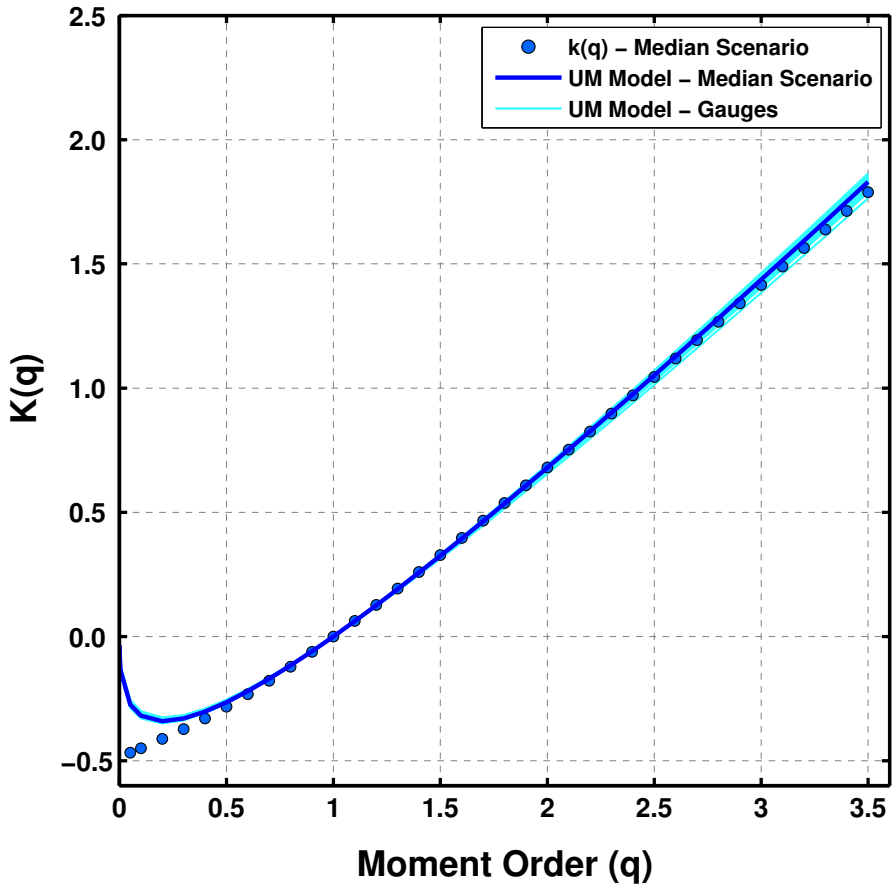

Fig. 8 Variation of the scaling exponent $k(q)$ with the moment order q. The filled circles represent $k(q)$s obtained from the linear regression of median trace moments of Figure 7, whereas the thick solid line represents corresponding fitted universal multifractal (UM) model. The thin lines represent UM models fitted to trace moments of each gauge series.

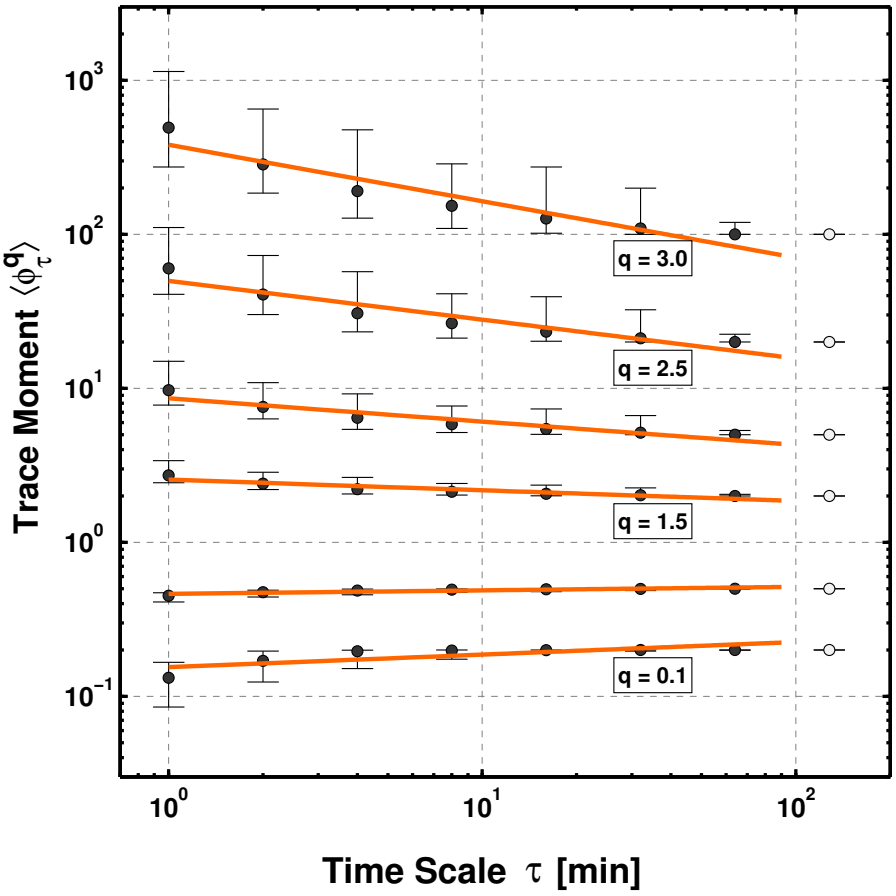

Fig. 9 Temporal scale-invariance in trace moments obtained from 1-minute data for different moment orders. The circles represent median value (out of 111 values) of trace moments, and the vertical bars indicate inter-event variability. The solid lines represent power laws fitted to the filled circles.

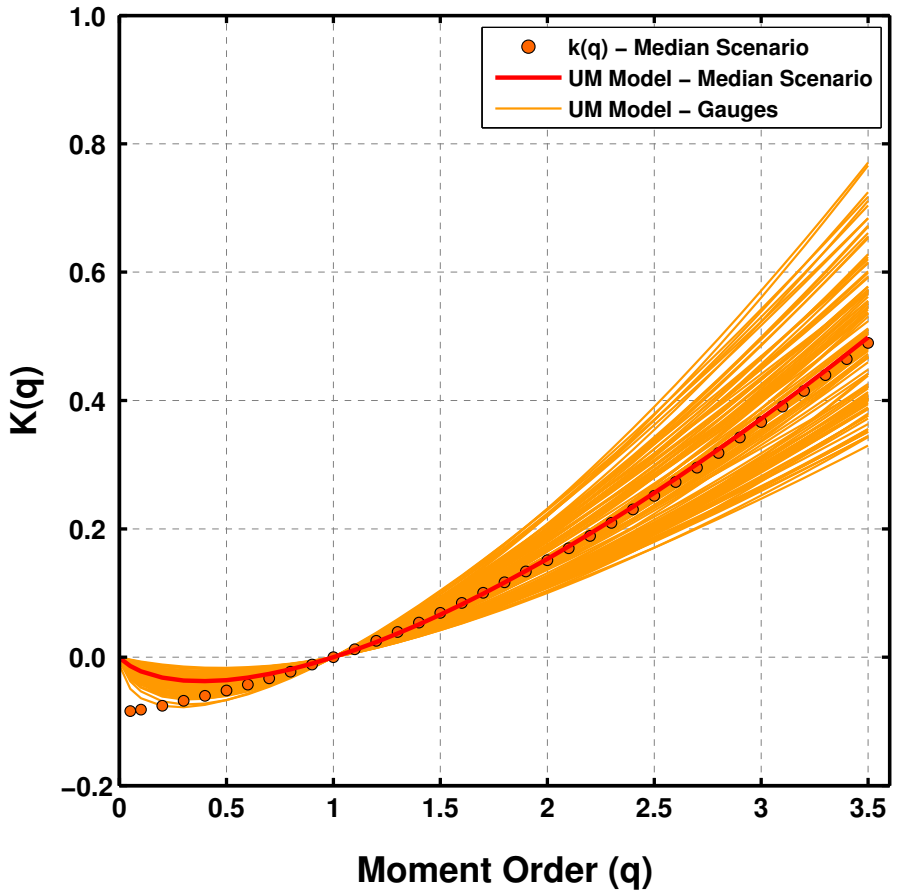

Fig. 10 Variation of the scaling exponent $k(q)$ with the moment order q. The filled circles represent $k(q)$s obtained from the linear regression of median trace moments of Figure 9, whereas the thick solid line represents corresponding fitted universal multifractal (UM) model. The thin lines represent UM models fitted to trace moments of each event.